Porous Polymer Films with Gradient-Refractive-Index Structure for Broadband and Omnidirectional Antireflection Coatings

ARTICLE *in* ADVANCED FUNCTIONAL MATERIALS · JANUARY 2010

Impact Factor: 11.81 · DOI: 10.1002/adfm.200901052

4 AUTHORS, INCLUDING:

Longjian Xue
Wuhan University
36 PUBLICATIONS **779** CITATIONS

SEE PROFILE

ADVANCED FUNCTIONAL MATERIALS
www.afm-journal.de

Porous Polymer Films with Gradient-Refractive-Index Structure for Broadband and Omnidirectional Antireflection Coatings

By *Xiao Li, Junpeng Gao, Longjian Xue,* and *Yanchun Han**

Porous polymer films that can be employed for broadband and omnidirectional antireflection coatings are successfully shown. These films form a gradient-refractive-index structure and are achieved by spin-coating the solution of a polystyrene-block-poly(methyl methacrylate) (PS-b-PMMA)/PMMA blend onto an octadecyltrichlorosilane (OTS)-modified glass substrate. Thus, a gradient distribution of PMMA domains in the vertical direction of the entire microphase-separated film is obtained. After those PMMA domains are removed, a PS porous structure with an excellent gradient porosity ratio in the vertical direction of the film is formed. Glass substrates coated with such porous polymer film exhibit both broadband and omnidirectional antireflection properties because the refractive index increases gradually from the top to the bottom of the film. An excellent transmittance of >97% for both visible and near-infrared (NIR) light is achieved in these gradient-refractive-index structures. When the incident angle is increased, the total transmittance for three different incident angles is improved dramatically. Meanwhile, the film possesses a color reproduction character in the visible light range.

1. Introduction

Antireflection (AR) coatings are needed to maximize the transmission of light through optical surfaces and to achieve high contrast and brightness in display devices, such as cathode ray tubes (CRTs), plasma display panels (PDPs), and liquid crystal devices (LCDs), and are useful for solar cells, lasers, other photovoltaic devices, and all kinds of optical lenses.[1] The principle of AR is the destructive interference between the reflected light from the air–coating and coating–substrate interfaces.[2] An ideal homogeneous AR coating should satisfy the following conditions: the thickness of the coating should be $\lambda/4$, where λ is the wavelength of the incident light; and $n_c = (n_a\, n_s)^{1/2}$, where n_c, n_a, and n_s are the refractive indices of the coating, air, and substrate, respectively. However, even when the AR coating meets the above conditions, an effective 0% reflection is achieved only at a specific wavelength because of the uniform refractive index throughout the whole film. The required optical thickness is only appropriate for a narrow spectral width because destructive interference occurs at a particular wavelength. The wavelength of the maximum transmittance shifts to the infrared region by increasing the film thickness.

As for broadband AR coatings, the critical problem is to avoid a sharp refractive index variation between the air and substrate interfaces. Excellent broadband AR films cannot be achieved if the refractive index is uniform throughout the entire thickness of the film. The refractive index of the film should gradually increase from the top to the bottom of the film. According to optical theory, conditions to design a broadband AR coating, namely a multilayer film with a different refractive index for each layer, are:[3] 1) the optical thickness of each layer has to be at least one quarter of the wavelength of the incident light. 2) The regular arrangement of the reflective indices of each layer should be $n_g > n_k > n_{k-1} \ldots > n_0$, where n_g and n_0 are the reflective indices of the substrate and of air, respectively, and k is the sequence number of the layer. 3) It can be verified theoretically that for suitable refractive indices, the n_k film can achieve 0% reflection at the λ_k wavelength. As such, the reflective index of a multilayer stack should satisfy the equation: $n_1/n_0 = n_2/n_1 = \ldots\ldots = n_k/n_{k-1} = n_g/n_k$. Herein we designed a gradient-refractive-index porous film by extending the number of intermediate index layers to infinity, thus breaking the air–substrate index discontinuity into smaller and smaller steps. Therefore, the discontinuity of the uniform refractive index film was replaced by a continuous transition from a low to a high refractive index, and this gradient-refractive-index AR coating displays visible to near-IR (NIR) antireflection at both normal and oblique incident angles.

Over the last years, many approaches to fabricate broadband antireflection films have achieved an ideal AR efficiency in both the visible and NIR light ranges. For example, an array of conical protuberances with sinusoidal profiles was made by replicating fly eyes,[4] reactive ion etching (RIE) processes have also been used,[5–7] as well as arraying of SiO_2 microspheres,[8] and the

[*] Prof. Y. Han, X. Li, Dr. J. Gao, L. Xue
State Key Lab of Polymer Physics and Chemistry
Changchun Institute of Applied Chemistry
Chinese Academy of Sciences
Graduate School of the Chinese Academy of Sciences
5625 Renmin Street, Changchun 130022 (P.R. China)
E-mail: ychan@ciac.jl.cn

DOI: 10.1002/adfm.200901052

heteroepitaxial growth of nanorods.[9] The refractive index between the air and substrate sides of these structures can be varied gradually. The oblique-angle deposition of indium tin oxide (ITO) and vapor deposition of materials with different refractive indices have also been used to achieve graded-refractive-index structures.[10,11]

Compared to inorganic materials, polymeric materials have great practical value and wide applications in antireflection coatings, because they possess the ability of adhering to the flexible substrate and the advantage of easy large-area processing. Many approaches for the fabrication of porous polymer films to achieve ideal AR efficiency have been proposed. The transmittance in the visible-light range of a microphase-separated film by removing one component can reach values as high as 99.5%.[12,13] A nanoporous multilayer film processed by the breath-figure method and having a gradual porosity ratio for each layer showed low reflection in the NIR light range (900–2200 nm).[14] Zhang et al. have also demonstrated excellent AR in the visible and NIR light range of polyelectrolytes and charged colloidal particles assembled by a layer-by-layer (LBL) technique.[15] However, all of the current AR coatings have limitations in extending the spectral range of the transmittance. Moreover, the effect of the incident angle, namely the fact that the light transmittance at different incident angles deviates from that at normal incidence, is ignored.[8]

The above-mentioned AR films pose considerable advantages of transmittance in either the visible- or the NIR light range, but there are two problems: 1) present AR coatings cannot simultaneously satisfy both the visible-light range (400–800 nm) and the NIR-light range (800–2200 nm). As such, color reproduction cannot be achieved at the same time. The spectral components of the reflection from an uncoated optical surface are identical, which means that it reflects all light wavelengths in the same manner and the substrate, thus, appears to be white. The reflection from a homogeneously coated optical surface, on the other hand, is selective towards specific wavelengths, so the film displays a high transmittance only in a narrow wavelength range and the real color is destroyed. When several optical devices with spectral selectivity are linked into an overall optical system, the effect of enhanced transmittance destroys the real color completely. 2) The antireflection is incident-angle dependent. At normal incident angle, maximal light transmittance is obtained through uniform-refractive-index AR coatings. If the incident angle is larger than 30°, the reflection character will be changed enormously by the polarization effect. So it is a significant challenge to fabricate an AR coating for broadband omnidirectional antireflection and at the same time trying to reproduce the real color.

In this paper, we designed a porous film with gradually increasing refractive index from the top to the bottom of the film and a broadband omnidirectional antireflection and real-color reproduction is demonstrated. Our approach is simply based on spin-coating of a solution of a polystyrene-block-poly(methyl methacrylate) (PS-b-PMMA)/PMMA blend onto a modified glass substrate. In this way a graded distribution of PMMA domains in the vertical direction of the entire microphase separated film was achieved, without the need for multiple steps in the film preparation nor for post treatments, such as annealing at temperatures higher than the polymer glass transition temperature. After the PMMA component was removed, the porous film showed excellent broadband transmittance higher than about 97% in both the visible-light (400–800 nm) and NIR-light (800–2000 nm) wavelength ranges. For incident

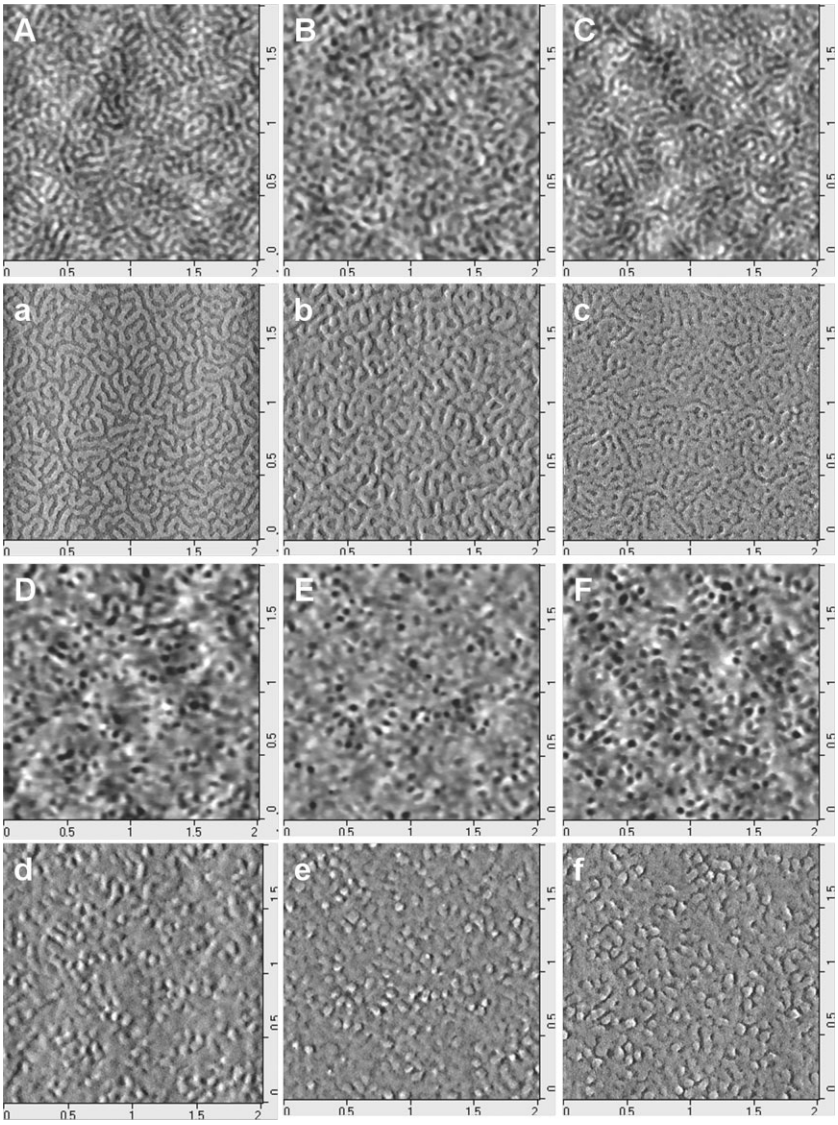

Figure 1. AFM topographic and phase images of A,a) PS-b-PMMA and B,b) PS-b-PMMA/PMMA in a single solvent (THF) at 27 mg mL^{-1}; C,c) PS-b-PMMA in mixed solvents (THF and TOL) at 27 mg mL^{-1} and PS-b-PMMA/PMMA in mixed solvents (THF and TOL) at D,d) 18 mg mL^{-1}; E,e) 27 mg mL^{-1}; and F,f) 36 mg mL^{-1}.

angles between 0° and 60° this porous film showed higher transmittance (increased by ca. 3%) than bare glass substrates. Because our gradient-refractive-index optical surface was not wavelength selective, the film also showed color reproduction at the same time.

2. Results and Discussion

2.1. Porous Polymer Films with Gradient-Porosity-Ratio Structures

To display broadband AR, the refractive index of the film coated on the substrate should not exhibit any sharp boundaries throughout the entire film. So the inner structure of a film with gradient-refractive-index, which is achieved by a porosity ratio gradually increasing from the bottom to the top of the film, is one of the best options. Here, a solution of PS-b-PMMA copolymer and PMMA homopolymer and the modulation of the concentration of this solution were used to fabricate an ideal structure with PMMA domains gradually increasing from the top to the bottom. It can be seen that the as-cast PS-b-PMMA diblock copolymer film with THF as solvent showed a disordered worm-like pattern (Fig. 1A,a) because of fast solvent evaporation. Since PMMA has a higher modulus than the PS chain at room temperature, PMMA is brighter in atomic force microscopy (AFM) phase-contrast images.[16,17] By adding the homopolymer PMMA into the solution or using a mixed solvent, the film also showed disordered worm-like patterns, but the AFM phase images (Fig. 1B,b and Fig. 1C,c) showed that the PMMA domains at the film surface increased. When both the homopolymer PMMA was added and the mixed solvent was used, the worm-like pattern disappeared and the film surface was almost completely covered by PMMA domains (Fig. 1D,d, E,e, and F,f). Although the concentration changed from 18 mg mL^{-1} (Fig. 1D,d) to 27 mg mL^{-1} (Fig. 1E,e) and 36 mg mL^{-1} (Fig. 1F,f), the film surface morphology did not change much.

After the PMMA block was degraded and washed, a porous film was obtained. The morphologies of these porous films are shown in Figure 2, which displays AFM height images from which the film surface roughness (RMS), the refractive index (n), and the pore volume (f_{pore}) were yielded. The pore volume in the film was calculated by:[18]

$$n^2 = n_{polymer}^2(1 - f_{pore}) + n_{air}^2 f_{pore} \quad (1)$$

where $n_{polymer}$, n_{air}, and f_{pore} are the refractive index of the polymer and air, and the pore volume fraction in the film, respectively. The copolymers gained by using a single solvent (THF), by adding the homopolymer, or by using the mixed solvent (Fig. 2a–c) showed almost the same surface morphology. However, the surface roughness increased dramatically as adding the homopolymer induced light scattering. When the mixed solvent was used, the pore volume was a little higher than that in Figure 2a, and the surface roughness also increased slightly. For films where both the homopolymer was added and a mixed solvent was used in different concentrations, the results are shown in Figure 2d–f. When the concentration was low (18 mg mL^{-1}), the film had a low pore density and could not cover the whole substrate. As the concentration increased, the pore volume decreased and the surface roughness increased, but the high RMS (36 mg mL^{-1}) also induced increasing light scattering. Only at a concentration of 27 mg mL^{-1}, an optimal surface roughness and pore volume were obtained. To compare the inner structure of these porous films, cross-sectional and top-view scanning electron microscopy (SEM) images of these films are shown in Figure 3. The film prepared by using a mixed solvent and a concentration of 27 mg mL^{-1} displayed a relatively compact structure (Fig. 3a,b). The size of the nanopores was not suitable for high transmittance. By adding the PMMA homopolymer and regulating the solution concentration, different structures and film thicknesses were obtained. After the PMMA domains were removed a relatively similar top-view is kept but the original structure collapsed, indicating that the film was too thin to have a gradient refractive index (Fig. 3c,d shows the results for the 18 mg mL^{-1} film). When the concentration was increased to 27 mg mL^{-1}, the film thickness increased to 225 nm and the protuberances on the film surface and the multilayer structure of the interpenetrating polymer network can be distinguished as shown in Figure 3e,f. When the concentration was increased to 36 mg mL^{-1} (Fig. 3g,h), the thickness of the film increased to 326 nm after the PMMA domains were removed. The top-view SEM image shows that the size of the

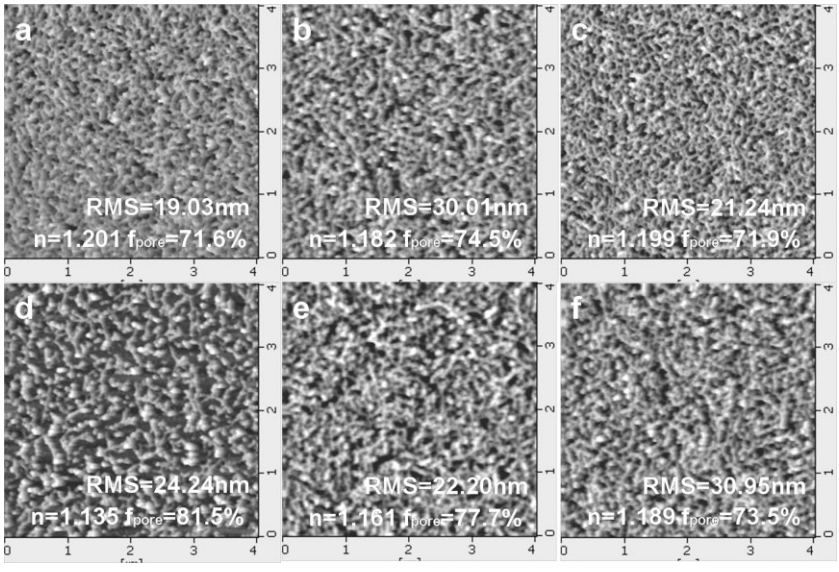

Figure 2. AFM height images after the films in Figure 1 were UV irradiated and then rinsed by acetic acid: a) PS-b-PMMA in single solvent (THF) at 27 mg mL^{-1}; b) PS-b-PMMA/PMMA in single solvent (THF) at 27 mg mL^{-1}; c) PS-b-PMMA in mixed solvents (THF and TOL) at 27 mg mL^{-1}; d–f) PS-b-PMMA/PMMA in mixed solvents (THF and TOL) at 18 mg mL^{-1}, 27 mg mL^{-1}, and 36 mg mL^{-1}, respectively.

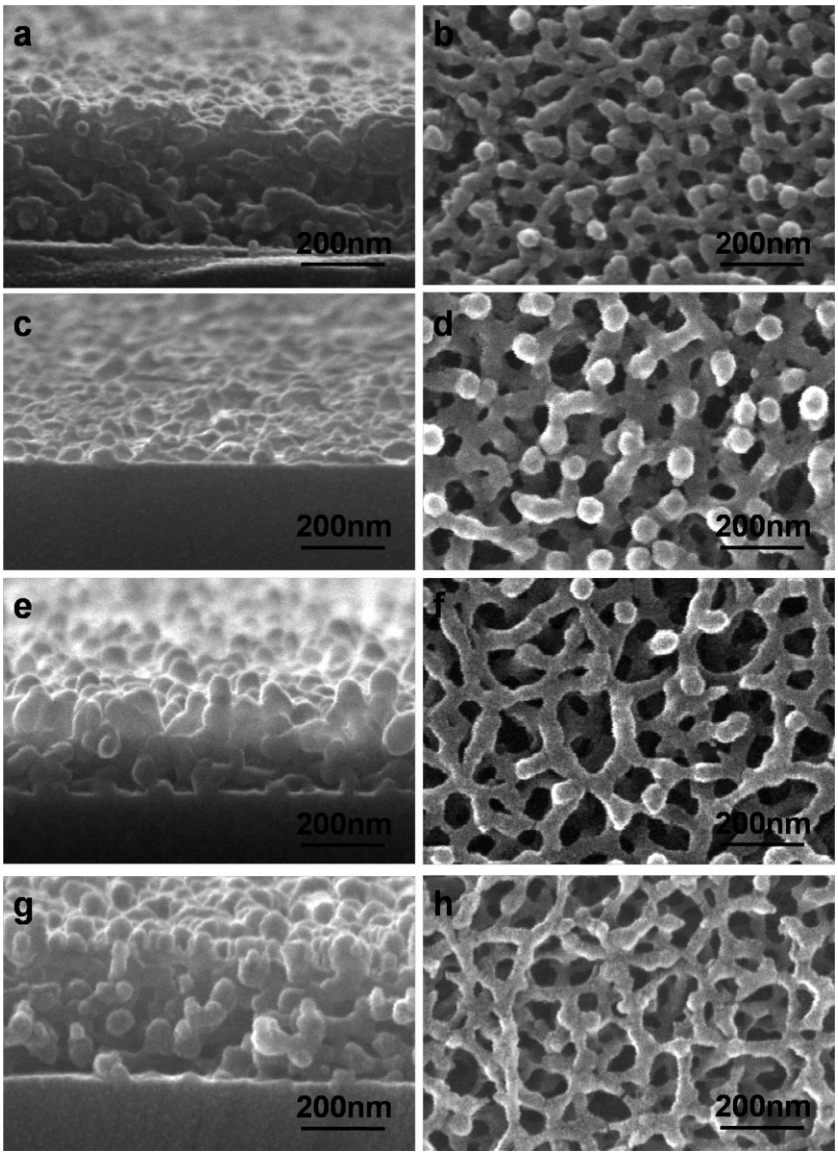

Figure 3. Cross-sectional and top-view SEM images of nanoporous films: a,b) PS-b-PMMA in mixed solvents (THF and TOL) at 27 mg mL^{-1} and PS-b-PMMA/PMMA in mixed solvents (THF and TOL) with different solution concentrations: c,d) 18 mg mL^{-1}, e,f) 27 mg mL^{-1}, and g,h) 36 mg mL^{-1}.

nanopores increased greatly and that the protuberances that induce light scattering in the visible light range have almost disappeared.

The gradient-porosity-ratio structure with suitable film thickness and surface morphology was obtained only at the concentration of 27 mg mL^{-1}. When the substrate with the AR film was irradiated with light at an oblique angle a purple colored film was obtained, as shown in Figure 4a. This color originated from the diffraction of light and interference effects because of the presence of the microstructure in the film at this certain angle. The incidence light at this angle was selectively reflected from the plane of the porous film in agreement with the Bragg equation.[19] The appearance of a purple color upon reflection was proof of the ideal structure in our AR film. The inner structure of the whole porous film resembles an interpenetrating polymer network. Figure 4b shows cross-sectional SEM images of the AR film, and no sharp boundaries can be found in the vertical direction of the film. Near the air–film surface a random array of conical protuberances can be seen, resembling moth compound eyes.[20] It is obvious that the porosity ratio of the top surface is higher than that of the bottom surface. The top surface of the film (Fig. 4c) exhibited a wide size distribution of the nanopores with a diameter ranging from 60 nm to 150 nm. The ascription of each pore to a specific layer cannot be made clearly, because the interpenetrating network was formed throughout the whole film by the residual PS chains. To determine the inner structure we treated the microphase-separated film before UV degradation with O_2 plasma, which etched the film from the surface with an accuracy on the nanometer scale.[21,22] We selected two etching rates and then removed the PMMA domains to obtain the inner-surface images. After O_2 plasma treatment for 60 s and 120 s, which corresponded to an etched thickness of around 83 nm (Fig. 4d) and around 165 nm (Fig. 4e), respectively, the nanopores became fewer and smaller than before O_2 plasma etching. The nanopores at the bottom of the film (Fig. 4f) were the smallest (10 nm–30 nm) and fewest, because the substrate prefers to absorb more PS chains. Therefore, we concluded that a gradient-porosity-ratio structure had been formed.

2.2. Proposed Mechanism of the Gradient-Porosity-Ratio Structure Formation

The gradient-index porous structure was obtained through modifying the surface energy of the substrate and using a mixed solvent. It is well known that the wetting behavior of block copolymers on a substrate is determined by the interfacial energy between the surface and each block of the copolymer. When symmetric PS-b-PMMA is cast on a glass substrate with OH groups on the surface, the PMMA block preferentially wets the substrate, while the PS block segregates to the air interface because of the presence of asymmetric boundary conditions.[23] After UV irradiating and rinsing with acetic acid, the film would peel off from the substrate easily because the adhesion between the substrate and the film was not strong enough. So our substrates were modified by octadecyltrichlorosilane (OTS) to retain alkyl chains on the surface and, thus, lower the surface energy. The surface tension of the OTS-modified substrate, PS block, and PMMA block are displayed in Table 1. The interfacial energy between the polymer and the substrate surface was

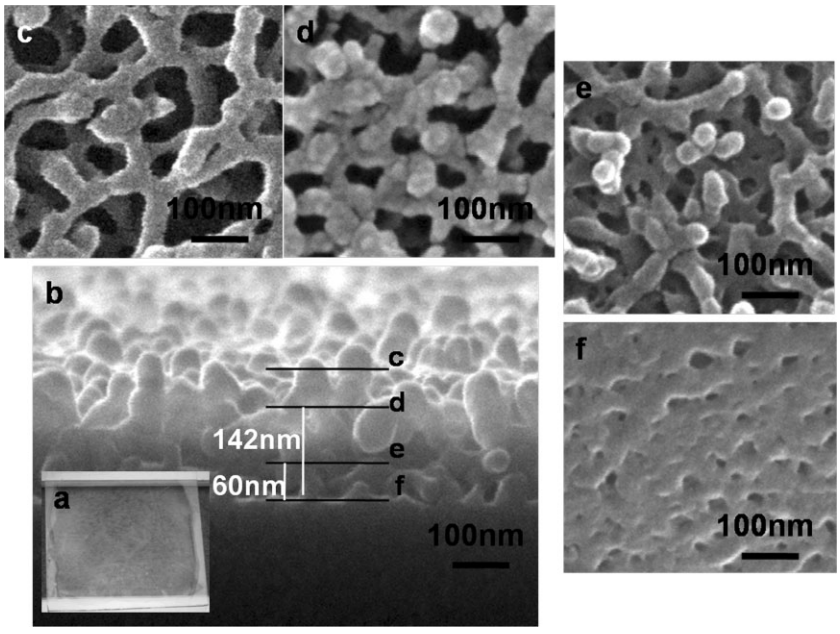

Figure 4. a) Photograph of the AR film in Figure 3e showing the purple color at certain incident angle. b) Cross-sectional and c–e) top-view SEM images before plasma etching (b,c) and after O_2 plasma etching (d,e) with different exposure times: d) 60 s, e) 120 s. The etching rate was determined to be ca. 1.4 nm s^{-1}. f) Bottom view of the nanoporous film in Figure 3e.

calculated using the following equation:[24]

$$\gamma_{1/2} = \gamma_1 + \gamma_2 - \frac{4\gamma_1^d\gamma_2^d}{\gamma_1^d + \gamma_2^d} - \frac{4\gamma_1^p\gamma_2^p}{\gamma_1^p + \gamma_2^p} \quad (2)$$

The interfacial energy between each block and OTS was: $\gamma_{PS/OTS} = 4.3\ mN\ m^{-1}$ and $\gamma_{PMMA/OTS} = 5.0\ mN\ m^{-1}$. Because PS has a lower interfacial energy than PMMA, the PS blocks in our copolymer preferred to wet the substrates covered with OTS, and the interaction between the PS porous film and the substrate was enhanced after the PMMA blocks were removed.

To strengthen the gradient distribution of the PMMA domains in the vertical direction of the whole film, a mixed solvent of tetrahydrofuran (THF, the boiling point is ca. 66 °C) and toluene (TOL, the boiling point is ca. 110 °C) was used. Without further annealing at high temperature, the initial nanostructure was formed by fast evaporation of nearly all of the THF during spin-coating but retaining most of the TOL in the system. With the help of the residual solvent, the copolymer (PMMA block) and homopolymer (PMMA) chains could move so that the distribution of the PMMA domains in the vertical direction of the entire film was adjusted slightly. Because the solvents continuously evaporated, the homopolymer PMMA chains preferred to migrate to the free surface because polymers with lower molecular weights have higher solubilities and, thus, the movement of the polymer chains is much easier. The formation process is illustrated in Scheme 1. Since the driving force for PMMA migrating was relatively weak, no lamellae or cylindrical morphology were obtained. Near the top surface more PMMA domains were found whereas near the substrate end the opposite situation was found because of the substrate surface modification with OTS. Therefore, the amount of PMMA microdomains throughout the film gradually increased from the substrate–film interface to the film–air interface. Furthermore, the size of the nanopores was increased by adding the homopolymer PMMA. After degrading and removing of the PMMA chains, a gradient-refractive-index film was obtained.

Table 1. The surface tension of the PS block, the PMMA block, and the substrate modified with OTS.

Specimen	γL(mN/m)	γd(mN/m)	γp(mN/m)
PS	32.1	26.7	5.4
PMMA	32.0	23.0	9.0
OTS-modified substrate	17.6	14.7	2.9

2.3. Broadband and Omnidirectional Antireflective Effect of the Film with Gradient-Porosity-Ratio Structure

The gradient-porosity-ratio structure with a continuous transition from low to high of the refractive index can satisfy visible to NIR antireflection at both normal and oblique incident angles. By modulating the concentration of the spinning solution, an optimal film thickness and suitable inner structure were obtained for the PS-b-PMMA/PMMA block copolymer film. Over the full light wavelength region (350–2000 nm), the transmittance of the AR film first increased with increasing film thickness until the film thickness reached 225 nm (the concentration was 27 mg mL^{-1}), then the transmittance began to decrease with increasing thickness. The variation in transmittance for four thicknesses is shown in Figure 5a. The bare glass substrate had a transmittance below 92% in the spectral range between 350 and 2000 nm. However, the transmittance of the glass substrates coated with an

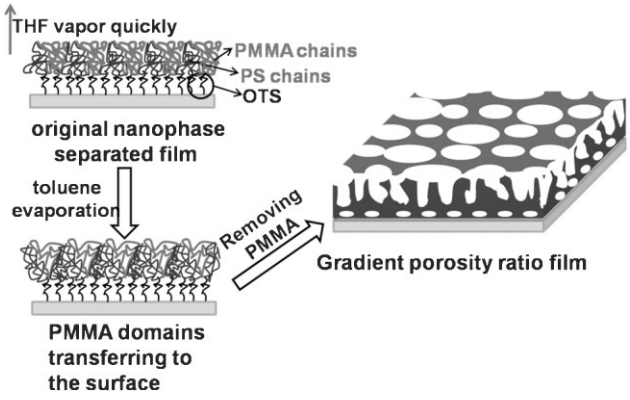

Scheme 1. Schematic representation of the gradient-porosity-ratio film-formation process.

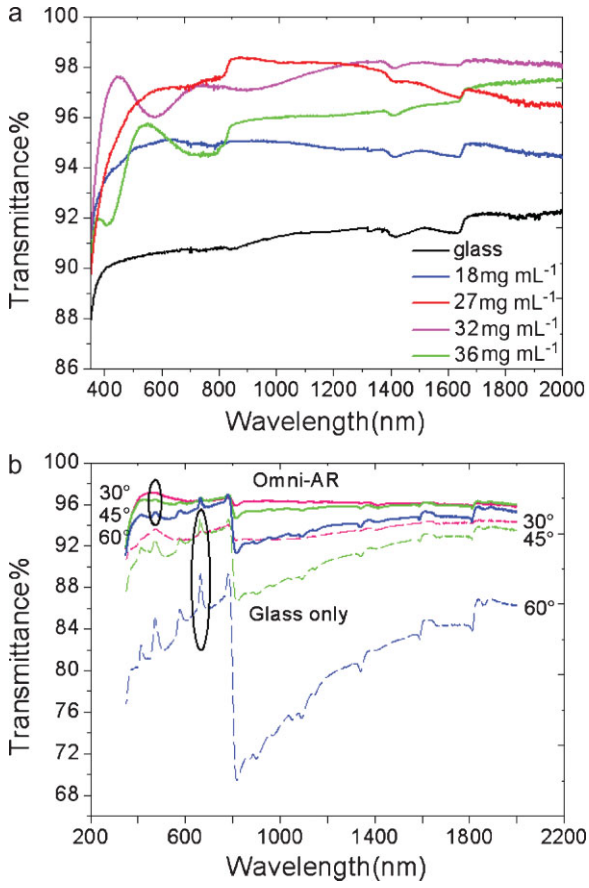

Figure 5. a) Transmission spectra of PS porous films with different thicknesses on the glass substrates at normal incidence. Note that both sides of the glass substrates are coated with a porous film. b) Angle-dependent transmittance of the glass at three different incident angles before and after the porous films were coated.

AR film was dramatically enhanced. The AR film of 225 nm (27 mg mL^{-1}) shows excellent broadband transmittance of about or over 97% in both the visible and NIR light range compared to AR films reported in the literature that only show good transmittance in either the visible light range or the NIR light range. Films with thicknesses of 71 nm (18 mg mL^{-1}) were too thin to achieve satisfactory AR over the whole spectral range. When the film thickness was increased to 287 nm (32 mg mL^{-1}), the transmittance in the visible light range decreased slightly and a maximum transmittance of 97.6% was achieved at a wavelength of 446 nm. For even higher thicknesses (326 nm, 36 mg mL^{-1}), the transmittance of both visible and NIR light decreased dramatically. Only a film thickness of 225 nm showed excellent broadband antireflection in both wavelengths: a transmittance above 96.5% for wavelengths of 500–800 nm, and even in the NIR range a transmittance of ca. 98% was achieved between 800 nm and 1400 nm and ca. 97% transmittance was obtained between 1400 nm and 2000 nm. These results give the above AR films great potential in many areas such as night-vision technology, output couples, dichroic mirrors, NIR sensors, and so forth.

The 225-nm film also showed oblique-angle light transmission which is called omnidirectional antireflection. It is well known that

Table 2. The changes of omni-AR transmittance at different incident angles.

	436 nm		1800 nm	
	Bare glass	Omni-AR	Bare glass	Omni-AR
30°	93.0%	97.1%	94.2%	95.9%
45°	91.5%	96.4%	94.5%	95.8%
60°	87.4%	94.8%	89.9%	94.6%

antireflection is incident-angle dependent since solar irradiation is generally received on a surface over a range of incident angles. Therefore, it is necessary to perform optical characterization at oblique incident angles not only to test the transmission in solar-energy components, but also that in AR optical devices. Many simulations on omnidirectional antireflectivity have been performed in previous research,[25,26] but materials that can realize this omnidirectional antireflectivity are scarce.[8,9] According to optical theory,[3] omnidirectional antireflection can easily be accomplished with a gradient-refractive-index film. Figure 5b shows the incident-angle-dependent transmittance measurements on our AR film compared to bare glass for contrast. For both the AR film and the bare glass substrate the transmittance decreases with increasing incident angle. However, it is clear that the transmittance of the AR film over the whole spectral range at the three different incident angles is dramatically higher than that of the bare glass substrate (Table 2), and with increasing incidence angle the transmittance of the AR film decreases much less than that of the bare glass substrate.

2.4. Color Reproduction Character

To appreciate the effect of the broadband AR property in the visible wavelength range, the optical images for a glass substrate with and without AR film that were exposed to sunlight are shown in Figure 6. The glass substrate on the left (without AR film) looks a little white and misty gray (Fig. 6a, left), and the words cannot be read clearly because of the ghost image from the light. Generally, uncoated substrates reflect all kinds of visible light, so that the different wavelengths mix, making the glass appear to be white. For oblique incident angles (Fig. 6b, left), the reflection of

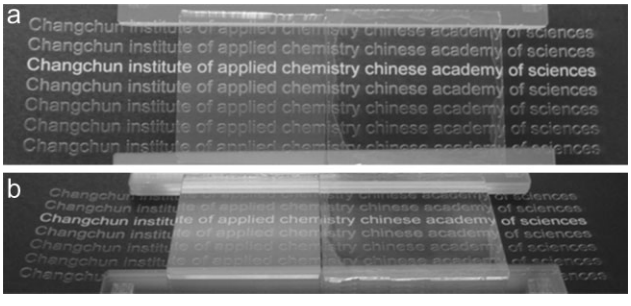

Figure 6. Photograph of glass substrates exposed to sunlight at a) normal incidence and b) oblique incidence. Left: a glass substrate without film coating. Right: a glass substrate with both sides covered with a PS porous film.

the bare glass slide was even stronger than at normal incidence. The glass looked white, the words can hardly be observed, and the real color was completely destroyed. On the contrary, the glass at the right hand side (with AR film) of Figure 6a and b demonstrates increased transparency and the real color of the words is reproduced phenomenally, even at oblique incident angles.

3. Conclusions

We have demonstrated a facile and effective method for preparing AR films with gradient refractive index. By spin-coating a solution of a polystyrene-block-poly(methyl methacrylate) (PS-b-PMMA)/PMMA blend onto an octadecyltrichlorosilane (OTS)-modified glass substrate, we obtained a gradient distribution of PMMA domains in the vertical direction of the entire microphase-separated film. After the PMMA domains were removed, a PS porous structure with excellent gradient porosity ratio in the vertical direction of the film was obtained. This graded film exhibited excellent broadband antireflection and omnidirectional antireflection in both the visible and NIR light range. In the visible light range the AR film possessed good color reproduction.

4. Experimental

Materials: The symmetric diblock copolymer of PS-b-PMMA ($M_{PS} = 133\,000$, $M_{PMMA} = 130\,000$, polydispersity $M_w/M_n = 1.10$) was purchased from Polymer Source Inc. The homopolymer PMMA with $M_w = 100\,000\,g\,mol^{-1}$ and octadecyltrichlorosilane (OTS, $CH_3(CH_2)_{17}SiCl_3$, 95%) were obtained from Sigma Aldrich Co. The solvents tetrahydrofuran, toluene, and acetic acid were purchased from Beijing Chemical, China. The water used was deionized water. The glass substrates were boiled in a piranha solution (7:3 (v/v) of 98% H_2SO_4/30% H_2O_2) for 30 min to remove any stains on the surface, then washed with deionized water, and dried with a nitrogen flow.

Modification of the Glass Substrates: The cleaned glass substrates were immersed in a 0.1% (v/v) solution of OTS in n-hexane. After 5 min they were removed from the OTS solution, washed with n-hexane for several times, and quickly dried under a N_2 flow.

Sample Preparation: The copolymer/homopolymer mixture was dissolved in a mixed solvent of THF and toluene (10 vol %) at four different concentrations (18, 27, 32, and 36 mg mL^{-1}). The solutions were spin-coated onto the modified glass substrates at 3500 rpm for 30 s. After all the solvent had completely evaporated, the whole film was irradiated by a UV lamp (model ZF-1, Shanghai Gucun Optic Instrument Factory, China) at the highest intensity at 365 nm for 3 h. The degraded PMMA chains were selectively removed by immersion in acetic acid for 1 h. Then the film was washed with deionized water for several times, and dried under a N_2 flow. To obtain the inner surface morphology, the specimen was etched for different times in a vacuum chamber with O_2 pressure of 100 mTorr and 100 W RF power. Under these conditions, the film was etched at a rate of ca. 1.4 nm s^{-1}. To measure the morphology at the bottom of the AR film, the porous film was hung in HF vapor for 5 min, and then floated onto water. The floated film was then picked up off the surface of the water by a hydrophobic silicon wafer with the bottom up.

Characterization: Atomic force microscopy (AFM) was used to study the surface topography of the spin-coated films. Images were obtained using a SPI3800N microscope (Seiko Instruments Inc., Japan) with a Si tip with a spring constant of 2 N m^{-1}. The cantilevers were operated slightly below their resonance frequency of around 72 kHz. The image acquisition was performed under ambient conditions. The AFM was used in tapping mode to reduce tip-induced surface degradation and sample damages. Imaging was conducted in the height mode.

The morphology and the cross-sectional images of the porous films were investigated by field-emission scanning electron microscopy (FE-SEM) using a Micro FEI Philips XL-30-ESEMFEG microscope.

Transmittance measurements in the spectral range of 350 to 2000 nm were performed using a Shimadzu UV-3600 spectrophotometer.

The thickness of the nanoporous films on the silicon wafer and the refractive indices were measured by spectroscopic ellipsometry over a wavelength range of 300–800 nm at a fixed incident angle of 70° using a UVISEL spectroscopic ellipsometer (Jobin Yvon, France).

The contact angles of deionized water and glycerol were measured on the OTS-modified glass substrate at ambient temperature using a DSA 10-MK1 (Krüss, Germany).

Acknowledgements

This research is subsidized by the National Natural Science Foundation of China (20621401, 50573077, 50773080).

Received: June 14, 2009
Revised: August 31, 2009
Published online: December 15, 2009

[1] a) Y. Zheng, K. Kikuchi, M. Yamasaki, K. Sonoi, K. Uehara, *Appl. Opt.* **1997**, *36*, 6335. b) R. Bilyalov, J. Stalmans, *J. Electrochem. Soc.* **2003**, *150*, G216. c) P. K. H. Ho, D. S. Thomas, R. H. Friend, N. Tessler, *Science* **1999**, *285*, 233. d) H. Ishikawa, Y. Honjo, K. Watanabe, *Thin Solid Films* **1999**, *351*, 212. e) H. Ohsaki, Y. Kokubu, *Thin Solid Films* **1999**, *351*, 1.
[2] H. A. Macleod, *Thin Film Optical Filters*, 2nd ed., Adam Hilger Ltd., Bristol, UK **1986**.
[3] Y. C. Lin, W. Q. Lu, *Thin Film Optical Theory* **1988**, Vol. *3*, Ch. 10.
[4] J. Y. Huang, X. D. Wang, Z. L. Wang, *Nanotechnology* **2008**, *19*, 025602.
[5] C. H. Sun, A. Gonzalez, N. C. Linn, P. Jiang, B. Jiang, *Appl. Phys. Lett.* **2008**, *92*, 051107.
[6] C. H. Sun, P. Jiang, B. Jiang, *Appl. Phys. Lett.* **2008**, *92*, 061112.
[7] W. L. Min, B. Jiang, P. Jiang, *Adv. Mater.* **2008**, *20*, 1.
[8] M. Tao, W. D. Zhou, H. J. Yang, L. Chen, *Appl. Phys. Lett.* **2007**, *91*, 081118.
[9] S. L. Diedenhofen, G. Vecchi, R. E. Algra, A. Hartsuiker, O. L. Muskens, G. Immink, E. P. A. M. Bakkers, W. L. Vos, J. G. Rivas, *Adv. Mater.* **2009**, *21*, 973.
[10] J. K. Kim, S. Chhajed, M. F. Schubert, E. F. Schubert, A. J. Fischer, M. H. Cho, J. Crawford, H. Kim, C. Sone, *Adv. Mater.* **2008**, *20*, 801.
[11] J. Q. Xi, M. F. Schubert, J. K. Kim, E. F. Schubert, M. Chen, S. Y. Lin, W. Liu, J. A. Smart, *Nat. Photonics* **2007**, *1*, 178.
[12] S. Walheim, E. Schäffer, J. Mlynek, U. Steiner, *Science* **1999**, *283*, 520.
[13] W. Joo, M. S. Park, J. K. Kim, *Langmuir* **2006**, *22*, 7960.
[14] M. S. Park, J. K. Kim, *Langmuir* **2005**, *21*, 11404.
[15] L. B. Zhang, Y. Li, J. Q. Sun, J. C. Shen, *Langmuir* **2008**, *24*, 10851.
[16] T. Xu, H. C. Kim, J. Derouchey, C. Seney, C. Levesque, P. Martin, C. M. Stafford, T. P. Russell, *Polymer* **2001**, *42*, 9091.
[17] U. Jeong, H. C. Kim, R. L. Rodriguez, I. Y. Tsai, C. M. Stafford, J. K. Kim, C. J. Hawker, T. P. Russell, *Adv. Mater.* **2002**, *14*, 274.
[18] T. C. Choy, *Effective Medium Theory*, Oxford University Press, New York, NJ **1999**.
[19] R. Anselmann, H. Winkler, *Adv. Eng. Mater.* **2003**, *5*, 8.
[20] P. B. Clapham, M. C. Hutley, *Nature* **1973**, *244*, 281.
[21] C. Harrison, M. Park, P. Chaikin, R. A. Register, D. H. Adamson, N. Yao, *Macromolecules* **1998**, *31*, 2185.
[22] S. Y. Yang, J. Park, J. Yoon, M. Ree, S. K. Jang, J. K. Kim, *Adv. Funct. Mater.* **2008**, *18*, 1371.
[23] K. Tanaka, A. Takahara, T. Kajiyama, *Macromolecules* **1996**, *29*, 3232.
[24] S. H. Wu, *J. Adhesion* **1973**, *5*, 39.
[25] W. D. Zhou, M. Tao, L. Chen, H. J. J. Yang, *Appl. Phys.* **2007**, *102*, 103105.
[26] A. G. Barriuso, J. J. Monzon, L. L. Sanchez-Soto, A. Felipe, *Opt. Commun.* **2007**, *270*, 116.